MINISTRY OF EDUCATION AND TRAINING

VIETNAM ACADEMY OF SCIENCE AND TECHNOLOGY

GRADUATE UNIVERSITY OF SCIENCE AND TECHNOLOGY

Cao Van Doan

NONLINEAR ELASTIC STATIC STABILITY OF SEVERAL GRAPHENE-REINFORCED COMPOSITE PLATES AND SHELLS SUBJECT TO MECHANICAL LOADS IN THE THERMAL ENVIRONMENT

SUMMARY OF DISSERTATION ON MECHANICS

Code: 9 52 01 01

Ha noi - 2024

The dissertation is completed at the Graduate University of Science and Technology, Vietnam Academy Science and Technology.

Supervisors:
1. Supervisor 1: Associate Prof., Ph.D. Vu Hoai Nam
2. Supervisor 2: Associate Prof., Ph.D. Đao Nhu Mai

Reviewer 1: Prof., Ph.D. Hoang Xuan Luong
Reviewer 2: Prof., Ph.D. Tran Van Lien
Reviewer 3: Ph.D. Tran Quoc Quan

The dissertation is examined by the Examination Board of the Graduate University of Science and Technology, Vietnam Academy of Science and Technology at.....

The dissertation can be found at:
1. Graduate University of Science and Technology Library
2. National Library of Vietnam

INTRODUCTION

1. The necessity of the dissertation

Graphene possesses unique mechanical and physical properties, including excellent electrical and thermal conductivity, as well as remarkable hardness and durability. A new composite, internationally known as Functionally Graded Graphene Reinforced Composites (abbreviated as FG-GRC), is obtained by reinforcing the polymer matrix with a certain volume fraction of graphene sheets. Advanced composites, such as FG-GRC, have attracted many research on the stability of structures made from these materials. The static stability of nonlinear elastic FG-GRC panels with complex curvature and the nonlinear elastic stability of FG-GRC shells reinforced by stiffener or containing Auxetic cores are important problems. However, the existing literature addressing these issues remains limited. Therefore, this dissertation focuses on studying the " ***Nonlinear elastic static stability of several graphene-reinforced composite plates and shells subject to mechanical loads in the thermal environment***" considering the stiffener system, auxetic cores, and the complex curvature of panels fabricated from FG-GRC.

2. The aims of the dissertation

Based on Donnell and HSDT theories, the static stability analysis of FG-GRC plates, shells reinforced by stiffeners or auxetic cores, and panels with complex curvatures under torsional loads, axial compression, and external pressure in thermal environments is conducted. The dissertation examines the influence of the stiffener system, geometrical characteristics, graphene distribution, elastic foundation, environmental temperature on the static stability of FG-GRC plates and shells.

3. Methodology

Theoretical methods

4. The main content of the dissertation

Includes introduction, 4 chapters, conclusion, list of author's scientific works and references.

CHAPTER 1. REVIEW

This chapter presents an overview of research on composite types, such as FGM, FG-CNTRC, FG-GRMMC, FG-GPLRC, and FG-GRC. Studies show that graphene increases the load-bearing capacity of composite structures, especially when the volume fraction of graphene is distributed more at the top and bottom of the shell. Based on the initial results in the work [135] of the thesis author and research team about the smeared stiffener technique, it can be seen that:

Based on Donnell and HSDT theory, it is necessary to continue to apply and develop this technique for structures of FG-GRC shells with reinforced FG-GRC stiffeners that can withstand loads in thermal environments.

The nonlinear elastic stability of FG-GRC shell reinforced by FG-GRC stiffener and an Auxetic core with a surrounding elastic foundation subjected to loads in a thermal environment has not yet been studied.

There is currently no research on the nonlinear elastic stability of plate structures, FG-GRC cylindrical panels with FG-GRC reinforced by stiffener, and the study of the stability of parabola panels and sinusoidal panels on nonlinear elastic foundations subjected to compressive loads, external pressure in the thermal environment, according to the HSDT.

The dissertation will focus on research to solve the above problems

CHAPTER 2. NONLINEAR ELASTIC STABILITY OF FG-GRC CYLINDRICAL SHELL AND TOROIDAL SHELL SEGMENTS REINFORCED BY STIFFENER, AUXETIC CORE

This chapter studies five problems based on Donnell shell theory. Specifically: 1) The stiffened FG-GRC toroidal shell segments in the thermal environment surrounded by the elastic foundation and subjected to torsional load. 2) Auxetic core FG-GRC toroidal shell segments have a surrounding elastic foundation subjected to torsional loads. 3) Auxetic core FG-GRC toroidal shell segments have a surrounding elastic foundation subject to mechanical load. 4) The stiffened FG-GRC cylindrical shell surrounding the

elastic foundation is subjected to torsional loads in thermal environments. 5) The stiffened FG-GRC cylindrical shell surrounding the elastic foundation is subjected to axial compression in a thermal environment. The significant new points of this chapter are the FG-GRC toroidal shell segment and FG-GRC cylindrical shell reinforced by an eccentric stiffer system, and the FG-GRC toroidal shell segment with an Auxetic core. Notably, the average circumferential stress is taken into account in the stress function for the first time in the toroidal shell segment that is subjected to torsional loads and surrounded by elastic foundations.

The internal force components are determined as follows

$$\begin{Bmatrix} N_x \\ N_y \\ N_{xy} \\ M_x \\ M_y \\ M_{xy} \end{Bmatrix} = \begin{bmatrix} A_{11} & A_{12} & 0 & B_{11} & B_{12} & 0 \\ A_{21} & A_{22} & 0 & B_{21} & B_{22} & 0 \\ 0 & 0 & A_{66} & 0 & 0 & B_{66} \\ B_{11} & B_{12} & 0 & D_{11} & D_{12} & 0 \\ B_{21} & B_{22} & 0 & D_{21} & D_{22} & 0 \\ 0 & 0 & B_{66} & 0 & 0 & D_{66} \end{bmatrix} \begin{Bmatrix} \varepsilon_x^0 \\ \varepsilon_y^0 \\ \gamma_{xy}^0 \\ -w_{,xx} \\ -w_{,yy} \\ -2w_{,xy} \end{Bmatrix} + \begin{Bmatrix} \Phi_{1x} \\ \Phi_{1y} \\ 0 \\ \Phi_{2x} \\ \Phi_{2y} \\ 0 \end{Bmatrix}, \quad (2.15)$$

where

$$\left(A_{ij}, B_{ij}, D_{ij}\right) = \left(A_{ijs}, B_{ijs}, D_{ijs}\right)_{[k]} + \left(A_{ijx}, B_{ijx}, D_{ijx}\right)_{[k]} + \left(A_{ijy}, B_{ijy}, D_{ijy}\right)_{[k]}, \quad (2.16)$$

and

$$\left(A_{ijs}, B_{ijs}, D_{ijs}\right)_{[k]} = \sum_{k=1}^{10} \int_{\Pi_k} Q_{ijs(k)} \left(1, z, z^2\right) dz, \quad (i, j = 1,2,6), \quad (2.17)$$

$$\begin{bmatrix} A_{11x} & B_{11x} \\ B_{11x} & D_{11x} \end{bmatrix} = \sum_{k=1}^{10} \left\{ \begin{bmatrix} \hat{A}_{11} & \hat{B}_{11} \\ \hat{B}_{11} & \hat{D}_{11} \end{bmatrix} - \begin{bmatrix} \hat{A}_{12} & 0 & \hat{B}_{12} & 0 \\ \hat{B}_{12} & 0 & \hat{D}_{12} & 0 \end{bmatrix} \begin{bmatrix} \hat{A}_{22} & 0 & \hat{B}_{22} & 0 \\ 0 & \hat{A}_{66} & 0 & \hat{B}_{66} \\ \hat{B}_{22} & 0 & \hat{D}_{22} & 0 \\ 0 & \hat{B}_{66} & 0 & \hat{D}_{66} \end{bmatrix}^{-1} \begin{bmatrix} \hat{A}_{12} & \hat{B}_{12} \\ 0 & 0 \\ \hat{B}_{12} & \hat{D}_{12} \\ 0 & 0 \end{bmatrix} \right\} \quad (2.18)$$

where

$$\left(\hat{A}_{ij},\hat{B}_{ij},\hat{D}_{ij}\right)_{(k)}=\frac{b_x}{d_x}\int\limits_{\Delta(k)}Q_{ij(k)}\left(1,z,z^2\right)dz,\quad (i,j\ =\ 1,2,6).\qquad (2.19)$$

2.3.1. Toroidal shell segment and cylindrical shell subjected to torsional load

The average deflection expression is chosen in the form [145]

$$w=\xi_0+\xi_1\sin\left[\beta\left(y-\lambda x\right)\right]\sin\left(\alpha x\right)+\xi_2\sin^2\left(\alpha x\right).\qquad (2.29)$$

Substituting (2.28) into the deformation compatibility equation leads to

$$\begin{aligned}\bar{\varphi}=&I_1\cos\left(2\alpha x\right)+I_2\cos\left[2\beta\left(-\lambda x+y\right)\right]+I_3\cos\left[\beta y+\left(\alpha-\lambda\beta\right)x\right]\\&+I_4\cos\left[\beta y-\left(\beta\lambda+\alpha\right)x\right]+I_5\cos\left[\beta y-\left(3\alpha+\lambda\beta\right)x\right]\\&+I_6\cos\left[\beta y+\left(3\alpha-\lambda\beta\right)x\right]+\sigma_{oy}hx^2/2-\tau hxy,\end{aligned}\qquad (2.30)$$

where σ_{oy} is average circumferential stress.

The expressions for torsional load and maximum deflection obtained are

$$\tau=\frac{1}{8}\frac{T_1{\xi_1}^6+T_2{\xi_1}^4+T_3{\xi_1}^2+T_4}{T_5\left(K_1L\pi a+2V_7{\xi_1}^2+2V_9\right)^2},\qquad (2.41)$$

$$W_{\max}=\frac{T_6{\xi_1}^4+T_7{\xi_1}^3+T_8{\xi_1}^2+T_9\xi_1+T_{10}}{8\left(K_1L\pi a+2V_7{\xi_1}^2+2V_9\right)T_{11}},\qquad (2.44)$$

Combining Eqs. (2.41), (2.44), the relationship between load and deflection of shell subjected to torsional load will be presented.

2.3.2. The Toroidal shell segment and cylindrical shell subjected to axial compression

The average deflection expression is chosen in the form

$$w(x,y)=\xi_0+\xi_1\sin\alpha x\sin\beta y+\xi_2\sin^2\alpha x.\qquad (2.47)$$

Substituting (2.45) into the deformation compatibility equation leads to

$$\begin{aligned}\bar{\varphi}=&\varphi_1\cos 2\alpha x+\varphi_2\cos 2\beta y-\varphi_3\sin\alpha x\sin\beta y\\&+\varphi_4\sin 3\alpha x\sin\beta y-\sigma_{0y}hx^2/2-phy^2/2.\end{aligned}\qquad (2.49)$$

Compressive (tensile) load equation with nonlinear deflection component

$$p = \frac{J_{43}\xi_2^{\,3} + J_{44}\xi_2^{\,2} + J_{45}\xi_2 + J_{46}}{J_{41}\xi_2 + J_{42}}. \tag{2.58}$$

Dimensionless deflection equation $W_{\max}/h$

$$\frac{W_{max}}{h} = \frac{1}{h}\left(J_{38}p + \frac{\xi_2}{2} + \frac{J_{37}\left(\left(J_{40} - 2J_{34}p\right)\xi_2 + J_{39}p\right)}{2J_{32}\xi_2 + 2J_{33}} + J_{36} + \sqrt{\frac{\left(J_{40} - 2J_{34}p\right)\xi_2 + J_{39}p}{2J_{32}\xi_2 + 2J_{33}}} \right). \tag{2.60}$$

Combining Eqs. (2.58) and (2.60), the relationship of compressive (or tensile) load with shell deflection will be presented.

2.5. Numerical investigation and discussion

In this part, the five problems mentioned above are analyzed and investigated.

Fig. 2.10 shows the effect of the stiffener system on the $\tau - W_{\max}/h$ postbuckling curves of the FG-GRC toroidal shell segment subjected to torsional loading. Orthogonal stiffener shells have the largest load capacity, and the curve is the highest in the small deflection region. Fig. 2.12 shows that the curve of the FG-X shell is the highest and the load-bearing capacity of this shell is the greatest.

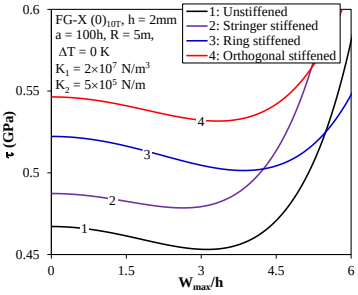

Fig 2.10. The effect of stiffener system on the $\tau - W_{\max}/h$ postbuckling curves of the FG-GRC toroidal shell segment.

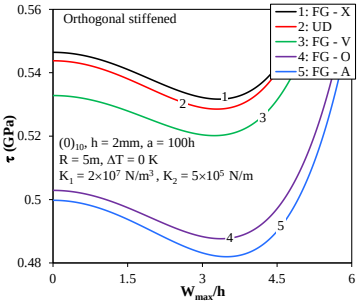

Fig 2.12. The $\tau - W_{\max}/h$ postbuckling curves of the five types FG-GRC toroidal shell segment.

Figure 2.22 compares the effects of the Auxetic core layer and the solid core layer on the $\tau - W_{\max}/h$ curve of the shells. It can be seen that the curve trends of the solid core and the Auxetic core shells are similar. Figure 2.27 presents the effect of longitudinal radius R on the $\tau - W_{\max}/h$ curve of two type shells. It is obvious that the torsional load capacity of the convex shell is much higher than that of the concave shell.

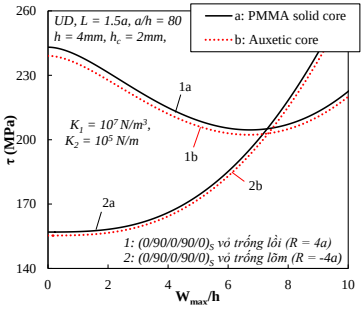

Fig 2.22. The effect of core layers on the $\tau - W_{\max}/h$ postbuckling curves of FG-GRC convex and concave shells.

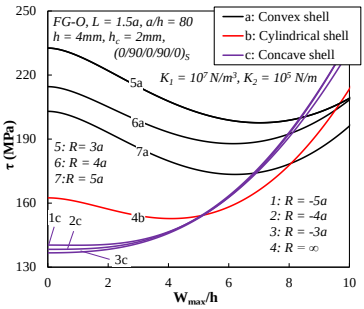

Fig 2.27. The effect of R on the $\tau - W_{\max}/h$ postbuckling curves of the FG-GRC convex and concave shells.

Table 2.16. The critical torsional load τ_{cr} (GPa) of FG-GRC cylindrical shell with and without stiffener ($L = 1.5a$, $a/h = 80$).

T = 300K				
Sample shell		Unstiffened	Stiffened	Effect (%)
UD	$(0)_{10T}$	0.287 (8;0.57)	0.536 (6;0.64)	86.76
FG-X	$(0)_{10T}$	0.299 (8;0.57)	0.526 (6;0.64)	75.92
FG-V	$(0)_{10T}$	0.257 (9;0.58)	0.548 (6;0.65)	113.23
FG-A	$(0)_{10T}$	0.257 (9;0.58)	0.442 (6;0.63)	71.98
FG-O	$(0)_{10T}$	0.242 (9;0.58)	0.478 (6;0.64)	97.52

Table 2.16 illustrates that the unstiffened FG-X cylindrical shell has the highest critical torsional load. However, the stiffened FG-V cylindrical shell exhibits the largest critical torsional load, while the critical torsional load of the stiffened FG-X cylindrical shell is smaller than that of the stiffened UD cylindrical shell. This highlights the significant impact of the stiffener system on the critical torsional load of the stiffened cylindrical shell.

Table 2.21 presents the effect of Auxetic core layer geometric parameters on the critical compressive and tensile loads of the FG-GRC toroidal shell segment. It is observed that the core layer's geometric parameters have an insignificant effect on the critical compressive and tensile loads of the shell. This result is the basis for design advanced structures with lightweight cores to reduce the mass of the sandwich structure.

Table 2.21. Effect of Auxetic core layer geometric parameters on critical compressive and tensile loads of FG-GRC toroidal shell segment (MPa, $L=1.5a$, $a/h=80$, $R=4a$, $h=4$ mm, $(0/90)_{5T}$)

FG-GRC		Critical compression load	Critical tenson load
$\chi_1=1$	UD	429.80 (7;1)	827.40 (1;9)
$\chi_2=0.1$	FG-X	411.37 (7;1)	813.45 (1;9)
$\gamma=15°$	FG-O	369.36 (7;1)	716.31 (1;10)
$\chi_1=2$	UD	429.37 (7;1)	827.39 (1;9)
$\chi_2=0.1$	FG-X	410.94 (7;1)	813.45 (1;9)
$\gamma=30°$	FG-O	368.93 (7;1)	716.26 (1;10)

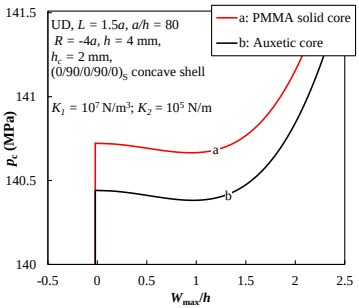

Fig 2.42. The effect of core layers on the $p_c - W_{\max}/h$ postbuckling curve of FG-GRC toroidal shell segment subjected to axial compression.

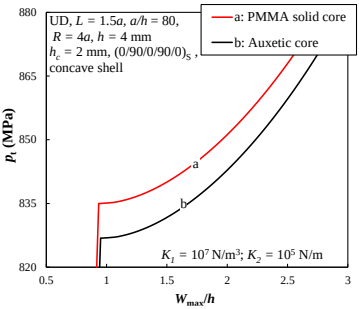

Fig 2.43. The effect of core layers on the $p_t - W_{\max}/h$ postbuckling curve of FG-GRC toroidal shell segment subjected to axial tension.

The effect of the core layers on the $p_c - W_{\max}/h$ and $p_t - W_{\max}/h$ postbuckling curve of the FG-GRC toroidal shell segment are presented in

Fig. 2.42 and Fig. 2.43. The critical load of the Auxetic core-shell is smaller than that of the solid core-shell, however, the curve trends are quite similar.

Table 2.25 shows the effectiveness of the stiffener on the critical load of FG-GRC cylindrical shells. As can be seen, the critical load of the unstiffened FG-X shell is the largest, while the critical load of the unstiffened FG-O shell is the smallest. The critical loads of stiffened UD shells are higher than those of the stiffened FG-X shells.

Table 2.25. The critical compression load p_{cr} (GPa) of the cylindrical shell FG-GRC ($L=1.5a$, $a=80h$, $h=2$ mm, $m=1$)

FG-GRC		T = 300 K		
		Unstiffened	Stiffened	Effect (%)
UD	$(0)_{10T}$	0.657(6;7)	1.060 (3;6)	61.34
	$(0/90/0/90/0)_s$	0.657(6;7)	1.059 (3;6)	61.19
	$(0/90)_{5T}$	0.656 (6;7)	1.059 (3;6)	61.43
FG-X	$(0)_{10T}$	0.681 (6;6)	1.050 (3;6)	54.19
	$(0/90/0/90/0)_s$	0.682 (6;6)	1.051 (3;6)	54.11
	$(0/90)_{5T}$	0.680 (6;6)	1.050 (3;6)	54.41
FG-V	$(0)_{10T}$	0.566 (6;7)	1.047 (3;6)	84.98
	$(0/90/0/90/0)_s$	0.566 (6;7)	1.048 (3;6)	85.16
	$(0/90)_{5T}$	0.565 (6;7)	1.047 (3;6)	85.31
FG-A	$(0)_{10T}$	0.585 (8;1)	0.915 (3;6)	56.41
	$(0/90/0/90/0)_s$	0.585 (8;1)	0.916 (3;6)	56.58
	$(0/90)_{5T}$	0.584 (8;1)	0.915 (3;6)	56.68
FG-O	$(0)_{10T}$	0.541 (7;6)	0.945 (3;6)	74.68
	$(0/90/0/90/0)_s$	0.540 (7;6)	0.946 (3;6)	75.19
	$(0/90)_{5T}$	0.540 (7;6)	0.945 (3;6)	75.00

Remarks of chapter 2

The important new point in this chapter is that the thesis has continued to apply and develop the smeared stiffener technique for FG-GRC stiffener, based on Lekhnitskii's idea and anisotropic classical beam theory. In particular, the average stress in the circumferential direction is considered for the first time in the stress function when calculating the stiffened FG-GRC toroidal shell segment surrounding the elastic foundation subjected to

torsional loads. From the numerical results, the thesis makes some notable comments as follows:

1. The stiffener system increases the critical torsional or axial compression and tensile load of the toroidal shells segment and cylindrical shells.

2. The FG-GRC convex shell has higher critical torsional and axial tensile compression loads compared to the FG-GRC concave shell. The sap-though phenomenon is apparent in toroidal shell segments, cylindrical shells under torsional loading, and cylindrical shells under axial compression. However, this phenomenon is not observed in auxetic core convex shells subjected to axial compressive loads.

3. The Auxetic core layer significantly reduces the structural mass, however, the critical load is not significantly reduced compared to the solid core case. This is the basis for designing advanced structures with lightweight cores to reduce the weight of sandwich structures.

The content of this chapter has been published in 6 papers published in prestigious international journals, which are works 1 to 6 in the author's list of scientific works related to the dissertation.

CHAPTER 3. NONLINEAR ELASTIC STABILITY OF STIFFENED FG-GRC CYLINDRICAL PANELS AND PLATES USING HSDT

In this chapter, the thesis studies the nonlinear stability of FG-GRC cylindrical panels and plates subjected to axial compressive load and external pressure in a thermal environment. Specific: 1) The stiffened FG-GRC piezoelectric cylindrical panel on a linear elastic foundation subjected to axial compression in a thermal environment. 2) The stiffened FG-GRC cylindrical panel on a nonlinear elastic foundation subjected to axial compression in a thermal environment. 3) The stiffened FG-GRC piezoelectric plate under axial compression and external pressure. 4) The stiffened FG-GRC plate on a nonlinear elastic foundation subjected to axial compression and external pressure.

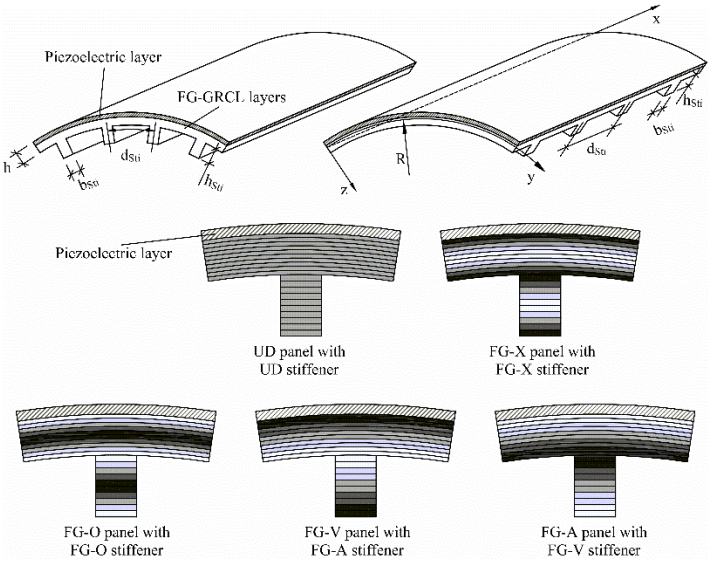

Fig 3.1. The shape and coordinate system of the stiffened FG-GRC piezoelectric panel

In this chapter, a new improved smeared stiffener technique for the higher-order shear deformable anisotropic stiffeners is presented. The new technique is based on the ideal of classical technique combined with the higher-order shear deformation theory for anisotropic beam taking into account the mechanical and thermal terms. The chapter investigates nonlinear stability for FG-GRC plates and panels under axial compressive load and external pressure using the nonlinear elastic foundation model [154]. The problems in this chapter are formulated based on HSDT, which considers the geometric nonlinearity according to von Kármán.

The solutions of deflection and rotations satisfying boundary conditions while utilizing the Galerkin method to establish relationships between loads and deflections.

The expression for internal force according to HSDT is

$$\begin{Bmatrix} N_x \\ N_y \\ N_{xy} \\ M_x \\ M_y \\ M_{xy} \\ T_x \\ T_y \\ T_{xy} \end{Bmatrix} = \begin{bmatrix} A_{11} & A_{12} & 0 & B_{11} & B_{12} & 0 & C_{11} & C_{12} & 0 \\ A_{12} & A_{22} & 0 & B_{12} & B_{22} & 0 & C_{12} & C_{22} & 0 \\ 0 & 0 & A_{66} & 0 & 0 & B_{66} & 0 & 0 & C_{66} \\ B_{11} & B_{12} & 0 & D_{11} & D_{12} & 0 & \hat{E}_{11} & \hat{E}_{12} & 0 \\ B_{12} & B_{22} & 0 & D_{12} & D_{22} & 0 & \hat{E}_{12} & \hat{E}_{22} & 0 \\ 0 & 0 & B_{66} & 0 & 0 & D_{66} & 0 & 0 & \hat{E}_{66} \\ C_{11} & C_{12} & 0 & \hat{E}_{11} & \hat{E}_{12} & 0 & L_{11} & L_{12} & 0 \\ C_{12} & C_{22} & 0 & \hat{E}_{12} & \hat{E}_{22} & 0 & L_{12} & L_{22} & 0 \\ 0 & 0 & C_{66} & 0 & 0 & \hat{E}_{66} & 0 & 0 & L_{66} \end{bmatrix} \begin{Bmatrix} \varepsilon_{0x} \\ \varepsilon_{0y} \\ \gamma_{0xy} \\ \phi_{x,x} \\ \phi_{y,y} \\ \phi_{x,y} + \phi_{y,x} \\ -\lambda\Gamma_1 \\ -\lambda\Gamma_2 \\ -\lambda\Gamma_3 \end{Bmatrix} - \begin{Bmatrix} \varphi_{1x} \\ \varphi_{1y} \\ 0 \\ \varphi_{2x} \\ \varphi_{2y} \\ 0 \\ \varphi_{4x} \\ \varphi_{4y} \\ 0 \end{Bmatrix}, \tag{3.9}$$

where

$$\begin{aligned} &A_{ij} = A_{ij}^S + A_{ij}^P + A_{ij}^{St},\ B_{ij} = B_{ij}^S + B_{ij}^P + B_{ij}^{St},\ D_{ij} = D_{ij}^S + D_{ij}^P + D_{ij}^{St} \\ &C_{ij} = C_{ij}^S + C_{ij}^P + C_{ij}^{St},\ \hat{E}_{ij} = E_{ij}^S + E_{ij}^P + E_{ij}^{St},\ L_{ij} = L_{ij}^S + L_{ij}^P + L_{ij}^{St}, \end{aligned} \tag{3.10}$$

and

$$\left(A_{ij}^S, B_{ij}^S, D_{ij}^S, C_{ij}^S, E_{ij}^S, L_{ij}^S\right) = \int_{-h/2+h_P}^{h/2} Q_{ijS}\left(1, z, z^2, z^3, z^4, z^6\right) dz, \tag{3.11}$$

$$\left(A_{ij}^P, B_{ij}^P, D_{ij}^P, C_{ij}^P, E_{ij}^P, L_{ij}^P\right) = \int_{-h/2}^{-h/2+h_P} Q_{ij}^P\left(1, z, z^2, z^3, z^4, z^6\right) dz, \tag{3.12}$$

$$\begin{aligned} &\begin{bmatrix} A_{ij}^{St} & B_{ij}^{St} & C_{ij}^{St} \\ B_{ij}^{St} & D_{ij}^{St} & E_{ij}^{St} \\ C_{ij}^{St} & E_{ij}^{St} & L_{ij}^{St} \end{bmatrix} = \begin{bmatrix} \bar{A}_{11} & \bar{B}_{11} & \bar{C}_{11} \\ \bar{B}_{11} & \bar{D}_{11} & \bar{E}_{11} \\ \bar{C}_{11} & \bar{E}_{11} & \bar{L}_{11} \end{bmatrix} - \begin{bmatrix} \bar{A}_{12} & 0 & \bar{B}_{12} & 0 & \bar{C}_{12} & 0 \\ \bar{B}_{12} & 0 & \bar{D}_{12} & 0 & \bar{E}_{12} & 0 \\ \bar{C}_{12} & 0 & \bar{E}_{12} & 0 & \bar{L}_{12} & 0 \end{bmatrix} \times \\ &\times \begin{bmatrix} \bar{A}_{22} & 0 & \bar{B}_{22} & 0 & \bar{C}_{22} & 0 \\ 0 & \bar{A}_{66} & 0 & \bar{B}_{66} & 0 & \bar{C}_{66} \\ \bar{B}_{22} & 0 & \bar{D}_{22} & 0 & \bar{E}_{22} & 0 \\ 0 & \bar{B}_{66} & 0 & \bar{D}_{66} & 0 & \bar{E}_{66} \\ \bar{C}_{22} & 0 & \bar{E}_{22} & 0 & \bar{C}_{66} & 0 \\ 0 & \bar{L}_{22} & 0 & \bar{E}_{66} & 0 & \bar{L}_{66} \end{bmatrix}^{-1} \begin{bmatrix} \bar{A}_{12} & \bar{B}_{12} & \bar{C}_{12} \\ 0 & 0 & 0 \\ \bar{B}_{12} & \bar{D}_{12} & \bar{E}_{12} \\ 0 & 0 & 0 \\ \bar{C}_{12} & \bar{E}_{12} & \bar{L}_{12} \\ 0 & 0 & 0 \end{bmatrix}, \end{aligned} \tag{3.13}$$

$$\left(\bar{A}_{ij},\bar{B}_{ij},\bar{D}_{ij},\bar{C}_{ij},\bar{E}_{ij},\bar{L}_{ij}\right)=\frac{b_{Sti}}{d_{Sti}}\int_{h/2}^{h/2+h_{Sti}} Q_{ij}^{St}\left(1,z,z^2,z^3,z^4,z^6\right)dz. \quad (3.14)$$

The deformation compatibility equation is obtained

$$\begin{aligned}\psi \equiv & A_{11}^{*}f_{,xxxx}+d_1 f_{,xxyy}+A_{22}^{*}f_{,yyyy}+w_{,xx}/R-\left(w_{,xy}\right)^2+d_3\phi_{x,xxx}\\ & +w_{,xx}w_{,yy}+w_{,xx}w_{0,yy}-2w_{,xy}w_{0,xy}+w_{,yy}w_{0,xx}+d_4\phi_{x,xyy}\\ & -C_{21}^{*}\lambda w_{,xxxx}+d_2 w_{,xxyy}-C_{12}^{*}\lambda w_{,yyyy}+d_5\phi_{y,xxy}+d_6\phi_{y,yyy}=0.\end{aligned} \quad (3.34)$$

The solutions of deflection and rotations and stress function are chosen as [144]

$$\begin{aligned} & w=W\sin\alpha x\sin\beta y,\quad w_0=\xi h\sin\alpha x\sin\beta y,\\ & \phi_x=\Phi_x\cos\alpha x\sin\beta y,\ \phi_y=\Phi_y\sin\alpha x\cos\beta y.\end{aligned} \quad (3.35)$$

$$f=f_1\cos 2\alpha x+f_2\cos 2\beta y+f_3\sin\alpha x\sin\beta y+\frac{1}{2}N_{x0}y^2+\frac{1}{2}N_{y0}x^2. \quad (3.36)$$

3.3.1. The stiffened FG-GRC panels and plates are subjected to external loads

The expression between the external pressure load q and $\bar{W}=W/h$ is obtained as follows

$$\begin{aligned}q=&q_1\left(2\xi+\bar{W}\right)\bar{W}\left(\xi+\bar{W}\right)+q_2\left(2\xi+\bar{W}\right)\bar{W}+q_3\bar{W}\left(\xi+\bar{W}\right)+q_4\bar{W}^3\\ &+q_5\bar{W}+\mu_2\frac{\varphi_{1y}}{R}+\left(\mu_1\frac{a_1\varphi_{1x}}{a_2}+\mu_2\frac{a_3\varphi_{1y}}{a_2}\right)\left(\xi+\bar{W}\right)h.\end{aligned} \quad (3.49)$$

Equation (3.49) is used to investigate the postbuckling curve of the stiffened FG-GRC panels and plate subjected to external pressure in a temperature environment.

3.3.2. The stiffened FG-GRC panels and plates are subjected to external loads and axial compression load

The axial load P_x is considered on edges $x=0,x=a$, $N_{x0}=-hP_x$, the equation relating load and deflection is obtained

$$a_{10}\bar{W}^3h^2+\frac{a_2q}{h}+\left(2\xi+\bar{W}\right)\bar{W}\left(\xi+\bar{W}\right)z_5+z_6\left(2\xi+\bar{W}\right)\bar{W}+z_7\bar{W}$$
$$+\mu_2z_4\left(\frac{a_2}{hR}+\left(\xi+\bar{W}\right)a_3\right)\varphi_{1x}-\mu_2\left(\frac{a_2}{hR}+\left(\xi+\bar{W}\right)a_3\right)\varphi_{1y} \quad (3.51)$$
$$+z_8\bar{W}\left(\xi+\bar{W}\right)+\left(\frac{a_2\mu_2z_1}{hR}+\left(\xi+\bar{W}\right)\left(a_3\mu_2z_1-ha_1\right)\right)P_x=0.$$

3.3.3. The stiffened FG-GRC under axial compression load

In this case $q=0$, with plate $R\to\infty$. At the first boundary condition FFFF $(\mu_2=0)$, from Eq. (3.51) lead to

$$P_x=\frac{1}{\left(\xi+\bar{W}\right)ha_1}\left(\begin{matrix}\left(2\xi+\bar{W}\right)\bar{W}\left(\xi+\bar{W}\right)z_5+z_6\left(2\xi+\bar{W}\right)\bar{W}\\ a_{10}\bar{W}^3h^2+z_7\bar{W}+z_8\bar{W}\left(\xi+\bar{W}\right)\end{matrix}\right). \quad (3.52)$$

At the second boundary condition FIFI ($\mu_2=1$). For perfect plate and panel $(\xi=0)$, Eq. (3.51) can be written

$$P_x=\frac{\left[\begin{matrix}\left(a_{10}h^2+z_5\right)\bar{W}^3+\left(z_6+z_8\right)\bar{W}^2+z_7\bar{W}\\ +\left(\frac{a_2}{hR}+\bar{W}a_3\right)\left(z_4\varphi_{1x}-\varphi_{1y}\right)\end{matrix}\right]}{-\left(\frac{a_2z_1}{hR}+\bar{W}\left(a_3z_1-ha_1\right)\right)}. \quad (3.54)$$

Equations (3.51), (3.52) and (3.54) are used to investigate the postbuckling curve and evaluate the postbuckling load-bearing capacity of stiffened FG-GRC cylindrical panels and plates subjected to axial compressive load in a temperature environment.

3.5. Numerical investigation and discussion

Table 3.3 shows the critical buckling compressive loads of the unstiffened and stiffened plate with various graphene distribution law types and the GRC direction arrangements. Notably, the numerical results show that the influence of the FG-GRC laminated stiffeners on the critical buckling loads is tremendously large. In the investigated results, it can be seen that the

critical loads of $x-$ and $y-$stiffened plates are equal. The critical load of stiffened FG-X plate is the highest in all investigation.

Table 3.3. Effect of graphene distribution cases types, the GRC direction arrangement, and direction stiffener system on the critical axial compression buckling load P_{cr} (MPa) of the FG-GRC laminated plates (FFFF, $a/b=1$, $\Delta T=0$K, $\xi=0$, $q=0$, $(m;n)=(1;1)$)

Tấm FG-GRC $a/h=20$		$(0)_{10T}$	$(0/90/0/90/0)_S$	$(0/90)_{5T}$
UD	Unstiffened	758.339	758.340	758.339
	$x-$Stiffener	1029.794	1029.995	1029.713
	$y-$Stiffener	1029.794	1029.995	1029.713
FG-X	Unstiffened	857.851	857.852	857.848
	$x-$Stiffener	1116.673	1116.951	1116.439
	$y-$Stiffener	1116.673	1116.951	1116.439
FG-O	Unstiffened	546.615	546.616	546.616
	$x-$Stiffener	782.857	783.098	783.214
	$y-$Stiffener	782.857	783.098	783.214
FG-V	Unstiffened	627.087	627.077	627.053
	$x-$Stiffener	953.010	952.950	952.397
	$y-$Stiffener	953.010	952.950	952.397
FG-A	Unstiffened	627.087	627.077	627.085
	$x-$Stiffener	797.062	797.469	797.253
	$y-$Stiffener	797.062	797.469	797.253

Fig. 3.5 displays the effect of stiffeners in $x-$ or $y-$direction on the P_x-W/h postbuckling curve of FG-X perfect plate. The curves of the stiffened plate are markedly higher than those of the unstiffened plates.

Figs. 3.7 indicate the influence of the graphene distribution laws (FG-X, UD, FG-V, and FG-O) on the P_x-W/h postbuckling curves of the $y-$stiffened laminated plates. Clearly, there is no bifurcation phenomenon with FG-GRC laminated plates in both cases of external pressure and of axial compression with pre-pressure. Similar to the critical buckling load results, the postbuckling curve P_x-W/h of FG-X type is the highest, opposite with FG-O type.

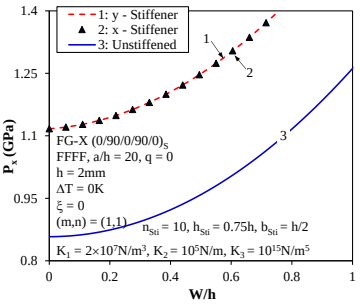

a) FG-GRC plate

Fig. 3.5. The effect of stiffener system on the $P_x - W/h$ postbucking curves of FG-GRC subjected to axial compression load.

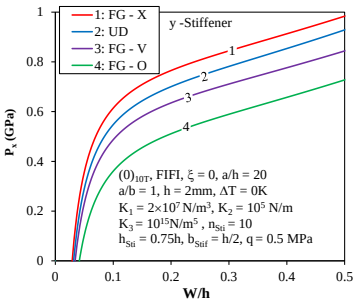

a) FG-GRC plate

Fig 3.7. The effect of graphene distribution laws on the $P_x - W/h$ postbucking curves of FG-GRC plate subjected to axial compression load and external pressures.

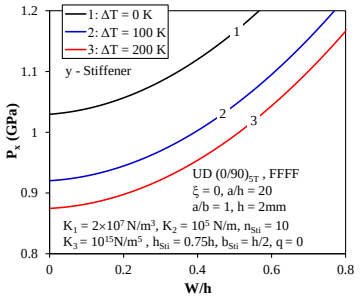

Fig 3.9. The effect of temperature on the $P_x - W/h$ postbuckling curve of FG-GRC plate subjected to axial compression load.

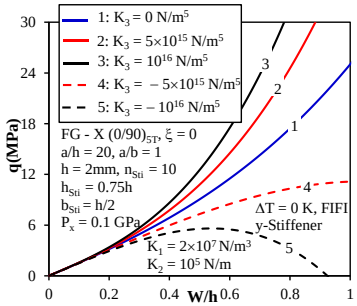

Fig 3.16. The effect of nonlinear modulus K_3 on the $q - W/h$ postbuckling curve.

Fig. 3.9 shows that the postbuckling curves $P_x - W/h$ of FG-GRC laminated plates declines during the thermal environment raises. The influences of nonlinear modulus K_3 on $q - W/h$ postbuckling curves of $y-$stiffened FG-GRC laminated plates are shown in Figs. 3.16. As can be seen, K_3 strongly effects to the trend of postbuckling curves.

Table 3.8 displays the P_{cr} of the unstiffened and stiffened FG-GRCL cylindrical panels with five graphene distribution law types and three graphene direction arrangements. For unstiffened panels, the P_{cr} of FG-X GRCL panels are the largest, and that of the FG-O GRCL panels is the smallest. However, for stiffened panels, the P_{cri} of FG-V GRC panels are the largest, and larger than one of FG-X GRC panels.

Table 3.8. Effect of graphene distribution law types, the graphene direction arrangement, and direction of the stiffener system on the P_{cr} (MPa) of the FG-GRCL cylindrical panels (FFFF, $a/b=1$, $a=20h$, $R=0.1\,\text{m}$, $\Delta T=0\,\text{K}$)

Panel FG-GRC		$(0)_{10T}$	$(0/90/0/90/0)_S$	$(0/90)_{5T}$
UD	Unstiffened	1132.730	1132.735	1132.923
	$x-$Stiffener [a]	2334.774	2331.225	2331.428
	$y-$Stiffener [b]	1305.782	1303.347	1301.835
FG-X	Unstiffened	1225.054	1225.065	1225.394
	$x-$Stiffener [a]	2358.357	2353.463	2354.648
	$y-$Stiffener [b]	1389.467	1387.049	1384.129
FG-O	Unstiffened	913.819	913.829	913.735
	$x-$Stiffener [a]	1937.087	1932.230	1931.244
	$y-$Stiffener [b]	974.272	969.954	970.228
FG-V	Unstiffened	973.794	973.976	974.296
	$x-$Stiffener [a]	2377.846	2372.953	2373.693
	$y-$Stiffener [b]	1173.034	1168.950	1166.382
FG-A	Unstiffened	1014.785	1014.602	1014.769
	$x-$Stiffener [a]	1769.637	1765.366	1765.552
	$y-$Stiffener [b]	1039.823	1037.312	1035.730

[a] Buckling mode (m,n) = (1,1)
[b] Buckling mode (m,n) = (2,1)

Fig. 3.19 show the effect of stiffeners in x or y direction on P_x-W/h postbuckling curve of FG-GRC cylindrical panels for the FFFF and FIFI boundary conditions, respectively. In general, both of these figures show the complex tendencies of the postbuckling curves of panels. The order of postbuckling strength of panels (unstiffened, $x-$stiffener, $y-$stiffener)

can change abnormally when changing from small deflection domain to large deflection domain.

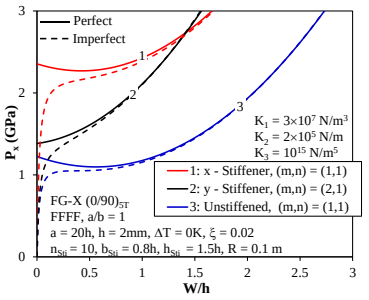

a) FFFF

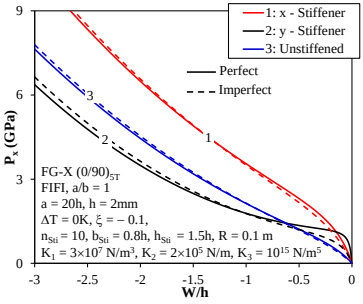

b) FIFI

Fig. 3.19. The effect of boundary condition and stiffeners in x or y directions on $P_x - W/h$ postbuckling curve.

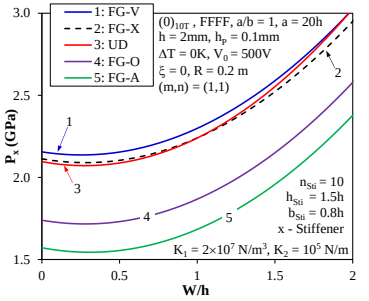

a) FFFF

Fig. 3.22. The effect of graphene distribution law on the $P_x - W/h$ postbuckling curve of the stiffened FG-GRC piezoelectric panel.

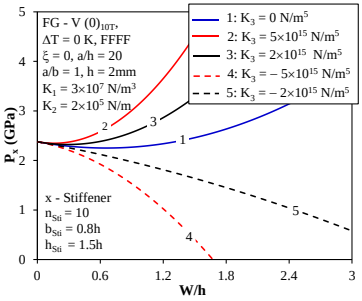

a) FFFF

Fig. 3.29. The effect of the nonlinear modulus K_3 on $P_x - W/h$ postbuckling curves.

Fig. 3.22 investigate the influence of five graphene reinforcement types (FG-X, UD, FG-O, FG-V, and FG-A) on the postbuckling behaviors of the stiffened (x-direction) FG-GRC piezoelectric cylindrical panels for the FFFF. As can be seen, the postbuckling curve of the FG-V graphene distribution type is the highest.

Fig. 3.29 shows the effect of nonlinear stiffness of foundation K_3 on the $P_x - W/h$ postbuckling curves of the stiffened(x -direction) FG-GRC cylindrical panels. Clearly, the values of nonlinear foundation stiffness K_3 significantly influence the $P_x - W/h$ postbuckling curves.

Remarks of chapter 3

From the above analysis results, the thesis presents the following general comments:

The stiffener system significantly increases the critical load of panels and plates. The snap-through phenomenon is observed in both perfect FG-GRC cylindrical panels and panels subjected to axial compression, without simultaneous external pressure.

The nonlinear stiffness K_3 does not alter the critical load of FG-GRC plates and cylindrical panels, however, it markedly influences the $P_x - W/h$ postbuckling curve trend.

The content of this chapter has been published in 4 papers published in international journals, which are works number 7 to 10 in the author's list of scientific works related to the dissertation.

CHƯƠNG 4. NONLINEAR BUCKLING AND POSTBUCKLING BEHAVIOR OF FG-GRC PARABOLIC AND HALF-SINUSOID SHALLOW IMPERFECT PANELS USING HSDT

This chapter presents research on two types of panels: parabolic panels and sinusoidal panels (defined by parabolic curve equations and sinusoidal half-cycle curve equations, respectively) subjected to external pressure and axial compressive loads in a thermal environment. The problems are formulated based on HSDT, taking into account von Kármán's geometric nonlinearity. Deflection and rotation angle solutions are chosen to satisfy the boundary conditions, and the Galerkin method is used to establish

the relationships between load and deflection, allowing the determination of the critical loads of the panel, if any.

The radius of curvature of the parabolic panel and the sinusoidal panel is

$$R_1 = \frac{\left(b^4 + 16H^2\left(b-2y\right)^2\right)^{3/2}}{8b^4H}, R_2 = \frac{\left(H^2\pi^2\left(\cos\left(y\pi/b\right)\right)^2 + b^2\right)^{3/2}}{bH\pi^2\sin\left(y\pi/b\right)}. \quad (4.2)$$

where H is the raise of panel.

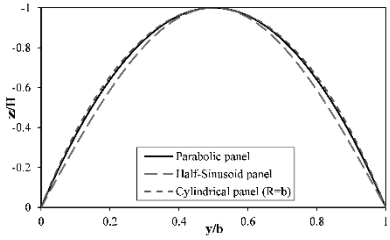

Fig. 4.1. Configuration example of mid-surface cross-section of half-sinusoid, parabolic, and cylindrical FG-GRC panels.

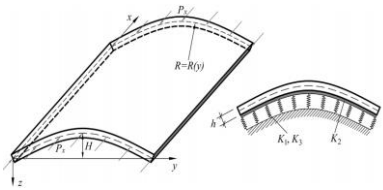

Fig. 4.2. Configuration of FG-GRC laminated panel resting nonlinear elastic foundation subjected to axial compression

The approximate stress function is chosen including both linear and non-linear components, as

$$f = f_{1(c,p,s)}\cos 2\alpha x + f_{2(c,p,s)}\cos 2\beta y + f_{3(c,p,s)}\sin\alpha x\sin\beta y + \frac{1}{2}N_{y0}x^2 + \frac{1}{2}N_{x0}y^2, \quad (4.3)$$

For parabolic and sinusoid panels, the radii of curvature are the complex functions, therefore, the exact form of stress functions cannot be determined. An approximation method is required to obtain the stress function in average forms in this chapter. Substituting Eq. (3.35) into Eq. (3.34) then, the amplitudes of stress function Eq. (4.3) in average sense can be obtained by applying the Galerkin procedure, as

$$\int_0^a\int_0^b \psi.\cos 2\alpha x\ dydx = 0, \int_0^a\int_0^b \psi.\cos 2\beta y\ dydx = 0, \int_0^a\int_0^b \psi.\sin\alpha x\sin\beta y\ dydx = 0. \quad (4.4)$$

where ψ is the expression in Eq. (3.34)

4.3.1. FG-GRC panel subjected to axial compression load

The expression for axial compressive load and deflection

$$P_x = \frac{\begin{pmatrix} z_{5(c,p,s)}\left(2\xi+\bar{W}\right)\bar{W} + z_{6(c,p,s)}\left(2\xi+\bar{W}\right)\bar{W}\left(\xi+\bar{W}\right) \\ +\mu_2\left(z_{4(c,p,s)}\varphi_{1x}-\varphi_{1y}\right)\left(\left(\xi+\bar{W}\right)x_{2(c,p,s)}+\frac{x_{11(c,p,s)}}{h}\right)+ \\ x_{7(c,p,s)}\bar{W}^3h^2 + z_{8(c,p,s)}\bar{W} + z_{7(c,p,s)}\bar{W}\left(\xi+\bar{W}\right) \end{pmatrix}}{\left(\mu_2 x_{2(c,p,s)}z_{1(c,p,s)} - hx_{1(c,p,s)}\right)\left(\xi+W_n\right)+\frac{\mu_2 x_{11(c,p,s)}z_{1(c,p,s)}}{h}}, \quad (4.10)$$

4.3.2. FG-GRC panel subjected to external pressure

The expression for external pressure load and deflection is as follows

$$q = \frac{-h\begin{pmatrix} q_{2(c,p,s)}\bar{W}\left(\xi+\bar{W}\right)+q_{1(c,p,s)}\left(2\xi+\bar{W}\right)\bar{W}\left(\xi+\bar{W}\right) \\ +\bar{W}c_{8(c,p,s)}+q_{4(c,p,s)}\bar{W}+\left(2\xi+\bar{W}\right)\bar{W}c_{7(c,p,s)}+ \\ \bar{W}^3h^2x_{7(c,p,s)}+q_{3(c,p,s)}\left(2\xi+\bar{W}\right)\bar{W} \end{pmatrix}}{x_{13(c,p,s)}}, \quad (4.15)$$

4.5. Numerical investigation and discussion

The critical buckling loads of parabolic, half-sinusoid, and cylindrical panels corresponding to the five distribution laws (FG-X, UD, FG-V, FG-A, and FG-O) and three arrangements at room temperature are presented in Table 4.3. The critical buckling loads of half-sinusoidal panels are notably higher than those of parabolic shell and cylindrical panels. Additionally, the critical buckling loads of parabolic panels slightly exceed those of cylindrical panels. Across all three panel types, the superiority of FG-X panels over those with other distribution laws remains obvious.

Table 4.3. Effect of graphene distribution and direction arrangement on the critical axial compression buckling load P_{cr} (MPa) (FFFF, $a/b=1$, $h=2mm$, $a=20h$, $H=1.5h$, $R=0.068167m$, $(m;n)=(1;1)$, $\Delta T=0K$)

$(0)_{10T}$	FG-X	UD	FG-O	FG-V	FG-A
Parabolic panel	1433.138	1349.139	1121.902	1152.995	1253.432
Half-sinusoid panel	1449.595	1365.970	1138.359	1168.504	1270.834
Cylindrical panel	1431.146	1347.102	1119.911	1151.111	1251.333

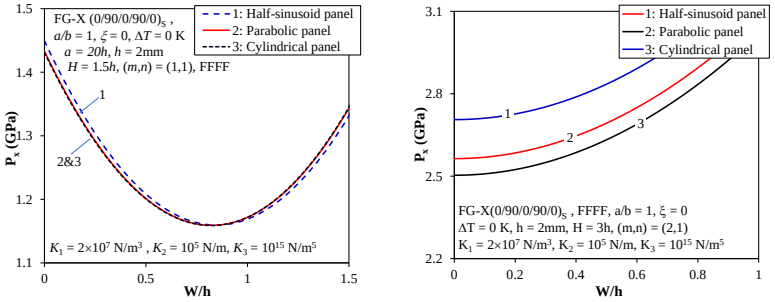

a) b)

Fig. 4.5. Comparison the $P_x - W/h$ postbuckling curves of three panel subjected to axial compression load.

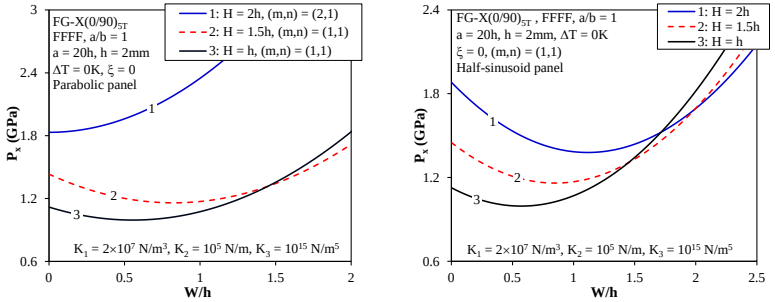

a) Parabolic panel b) Half-sinusoid panel

Fig. 4.8. The effect of the rise H on the $P_x - W/h$ postbuckling curves of panels.

The postbuckling curves of parabolic, half-sinusoid, and cylindrical panels are compared in Fig.4.5. The postbuckling curve trends in the three investigated cases can be shown to be similar, and the snap-through buckling

phenomenon is very obvious. As can be seen that the slight differences in postbuckling strength between three-panel types can be observed for the small value of the rise of panels H (Fig.4.5a). Oppositely, when the rise of panels increases, the differences in postbuckling curves of three-panel types become more significant (Fig.4.5b). The effect of the rise, denoted as H, on the critical load and $P_x - W/h$ curves of panel types is shown in Figure 4.8. As H increases, the critical load rises and changes the $P_x - W/h$ curve of the panel types.

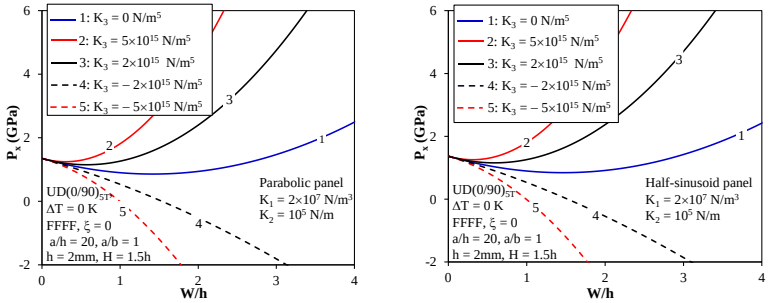

a) Parabolic panel b) Half-sinusoid panel

Fig. 4.11. The effect of the nonlinear modulus K_3 on $P_x - W/h$ postbuckling curves of parabolic and half-sinusoid panels.

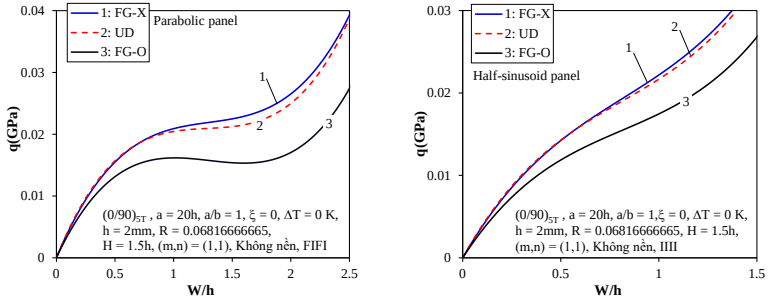

a) Parabolic panel b) Half-sinusoid panel

Fig. 4.14. The effect of graphene distribution on the $q - W/h$ postbuckling curve of panels subjected to external pressure.

Fig. 4.11 illustrates how the nonlinear stiffness K_3 influences the postbuckling curves of two different types of panels. The critical buckling load is unaffected by the values of K_3. However, the trend of the postbuckling curves is significantly altered. Fig. 4.14 evaluate the influences of the distributions (UD, FG-O, and FG-X) on the postbuckling behavior of the FG-GRC parabola and sinusoidal panels. The postbuckling bearing capacity of the FG-O type is the smallest and that of the FG-X type is the largest. In the case of parabola panels, the snap-through can be clearly observed for the FG-O panels.

Remarks of chapter 4

The thesis offers the following observations:

1. The snap-through phenomenon occurs in the positive deflection region with all three types of panels. The curve trend of the panel shells is the same in all surveys.

2. In the case of panels subjected to external pressure, bifurcation point loads are not observed in all investigated cases.

3. At the same H, the compression load capacity of the sinusoidal panel is the highest and the compression load capacity of the parabolic panel is the lowest.

The content of this chapter has been published in two papers, with one published domestically and the other in an international journal. These papers are listed as works 11 and 12 in the author's related scientific works.

CONCLUSION

The thesis has made new contributions as follows:

1. The thesis has analyzed the nonlinear stability of stiffened FG-GRC shells and plates, as well as FG-GRC toroidal shell segments with an Auxetic core, under torsional loads, axial compression, and external pressure in a thermal environment.

2. The thesis develops an improved smeared stiffener technique, applied to FG-GRC stiffeners within the framework of Donnell shell theory and HSDT, while considering thermal stress components in the stiffeners.

3. During the calculation process of the stiffened FG-GRC toroidal shell segment subjected to torsional loads with a surrounding elastic foundation, circumferential stress is considered in the stress function for the first time. Subsequently, following Galerkin analysis, the equations have been thoroughly used to accurately express the relationship between load and deflection.

4. The thesis also introduces a method to determine the average stress function, incorporating both linear and nonlinear components, in the nonlinear stability analysis of Parabolic panels and Sinusoidal panels under external pressure and axial compression in a thermal environment.

5. Nonlinear elastic foundations are considered into the analysis of stiffened FG-GRC plates, cylindrical panels subjected to combined mechanical loads, as well as in the problems of parabolic and half-sinusoidal panels subjected to axial compression in a thermal environment

THE LIST OF AUTHOR'S SCIENTIFIC WORKS RELATING TO THE CONTENT OF THE THESIS

1. **Cao Van Doan**, Vu Tho Hung, Nguyen Thi Phuong, Vu Hoai Nam, "*Torsional buckling and postbuckling behavior of stiffened FG-GRC toroidal shell segments surrounded by elastic foundation"*. International Journal of Computational Materials Science and Engineering, 2023, 12, 2350001.

2. Nguyen Thi Phuong, Vu Minh Duc, Dang Thuy Dong, **Cao Van Doan**, Pham Thanh Hieu, Vu Hoai Nam, *"An analytical approach of nonlinear buckling behavior of torsionally loaded auxetic core toroidal shell segments with graphene reinforced polymer coatings"*. Advanced Composite Materials, 2023, 32, 400–418.

3. Nguyen Thi Phuong, Vu Minh Duc, **Cao Van Doan**, Vu Hoai Nam, *"Nonlinear torsional buckling of functionally graded graphene-reinforced composite (FG-GRC) laminated cylindrical shells stiffened by FG-GRC laminated stiffeners in thermal environment".* Polymer Composites, 2021, 42, 3051–3063.

4. Vu Hoai Nam, Vu Minh Duc, **Cao Van Doan**, Nguyen Thi Thanh Xuan, Nguyen Thi Phuong, *"Nonlinear postbuckling behavior of auxetic-core toroidal shell segments with Graphene reinforced face sheets under axial loads"*. Archives of Mechanics, 2022, 74, 89–108.

5. Vu Hoai Nam., Nguyen Thi Phuong, Ho Si Lanh, Vu Minh Duc, **Cao Van Doan**, "*Nonlinear buckling analysis of stiffened FG-GRC laminated cylindrical shells subjected to axial compressive load in thermal environment*". Mechanics Based Design of Structures and Machines, 2023, 51, 3678–3694.
6. **Cao Van Doan**, Vu Hoai Nam, Nguyen Thi Phuong, "*Nonlinear Electro-Thermo-Torsional Buckling Analysis of Stiffened Functionally Graded Graphene-Reinforced Composite Laminated Toroidal Shell Segments*". Journal of Engineering Mechanics, 2023, 149, 04022106.
7. Nguyen Thi Phuong, Dang Thuy Dong, **Cao Van Doan**, Vu Hoai Nam, *"Nonlinear buckling of higher-order shear deformable stiffened FG-GRC laminated plates with nonlinear elastic foundation subjected to combined loads"*. Aerospace Science and Technology, 2023, 127, 107736.
8. Vu Hoai Nam, Dang Thuy Dong, **Cao Van Doan**, Nguyen Thi Phuong, *"Nonlinear Thermo-Electro-Mechanical Buckling of Higher-Order Shear Deformable Stiffened FG-GRC Laminated Plates"*. International Journal of Applied Mechanics, 2022, 14, 2250051.
9. Nguyen Thi Phuong, Dang Thuy Dong, **Cao Van Doan**, Vu Hoai Nam, *"Nonlinear buckling of stiffened FG-GRC cylindrical panels under axial compression with the uniformly distributed temperature variation"*. The European Physical Journal Plus, 2023, 138.
10. Vu Hoai Nam, Dang Thuy Dong, **Cao Van Doan**, Nguyen Thi Phuong, *"Nonlinear buckling of axially compressed FG-GRC stiffened cylindrical panels with a piezoelectric layer by using Reddy's higher-order shear deformation theory"*. Polymer Composites, 2022, 43,7952-7966.
11. Vu Hoai Nam, **Cao Van Doan**, Nguyen Thi Phuong, "*A new analytical approach to the nonlinear buckling and postbuckling behavior of functionally graded graphene reinforced composite laminated cylindrical, parabolic, and half-sinusoid shallow imperfect panels*". Polymer Composites, 2023, 1-18.
12. Nguyen Thi Phuong, **Cao Van Doan**, Vu Hoai Nam, "*Postbuckling analysis of externally pressured parabola, sinusoidal and cylindrical FG-GRCL panels using HSDT*". Journal of Science and Transport Technology, 2023, 3(2), 34-42.